HYDROLOGICAL PROCESSES
Hydrol. Process. (2008)
Published online in Wiley InterScience
(www.interscience.wiley.com) DOI: 10.1002/hyp.7021

Delineating runoff processes and critical runoff source areas in a pasture hillslope of the Ozark Highlands

M. D. Leh,[1] I. Chaubey,[2]* J. Murdoch,[1] J. V. Brahana[3] and B. E. Haggard[1]

[1] *Department of Biological and Agricultural Engineering, University of Arkansas, Fayetteville, AR 72701, USA*
[2] *Department of Agricultural and Biological Engineering and Department of Earth and Atmospheric Sciences, Purdue University, West Lafayette, IN 47907, USA*
[3] *Department of Geosciences, University of Arkansas, Fayetteville, AR, USA*

Abstract:

The identification of runoff contributing areas would provide the ideal focal points for water quality monitoring and Best Management Practice (BMP) implementation. The objective of this study was to use a field-scale approach to delineate critical runoff source areas and to determine the runoff mechanisms in a pasture hillslope of the Ozark Highlands in the USA. Three adjacent hillslope plots located at the Savoy Experimental Watershed, north-west Arkansas, were bermed to isolate runoff. Each plot was equipped with paired subsurface saturation and surface runoff sensors, shallow groundwater wells, H-flumes and rain gauges to quantify runoff mechanisms and rainfall characteristics at continuous 5-minute intervals. The spatial extent of runoff source areas was determined by incorporating sensor data into a geographic information-based system and performing geostatistical computations (inverse distance weighting method). Results indicate that both infiltration excess runoff and saturation excess runoff mechanisms occur to varying extents (0–58% for infiltration excess and 0–26% for saturation excess) across the plots. Rainfall events that occurred 1–5 January 2005 are used to illustrate the spatial and temporal dynamics of the critical runoff source areas. The methodology presented can serve as a framework upon which critical runoff source areas can be identified and managed for water quality protection in other watersheds. Copyright © 2008 John Wiley & Sons, Ltd.

KEY WORDS runoff; saturation excess runoff; infiltration excess runoff; runoff source area; GIS

Received 21 August 2006; Accepted 22 January 2008

INTRODUCTION

Storm runoff generation is a non-linear process that has surface and subsurface components. This has led to a number of runoff generation concepts, namely the Horton (1933) overland flow concept, the partial area concept (Betson, 1964) and the variable source area concept (Hewlett and Hibbert, 1967). While the runoff generation process at a particular location within a watershed could be a combination of these processes depending on climate, geology, topography, soil characteristics and rainfall patterns, studies have found that limited (less than 10%) portions of a watershed can contribute disproportionately large runoff amounts at the downslope end of the watershed (Freeze, 1974).

Large amounts of storm runoff from a catchment has implications for water quality, flood control and watershed management. For example, storm runoff plays a major role in phosphorous (P) transport and diffuse P pollution is a major contributor to freshwater systems. The role of P in accelerating eutrophication in freshwater systems was recognized over three decades ago (Schindler *et al*., 1971), and as a result, P transport has become a focus of water quality research. For hillslope watersheds, Pionke *et al*. (1997) reported that approximately 10% of a watershed area may contribute up to 90% of the annual P loads from that watershed. Although the relationship between runoff generation and P transport has been recognized for a decade (Zollweg *et al*., 1995; Gburek and Sharpley, 1998), there is a need to accurately identify and delineate critical areas (known as runoff source areas) of a watershed that may contribute heavily to runoff and nutrient transport. Identification of critical runoff source areas has many levels of importance to water resource managers and is of critical importance to the south-eastern USA. Runoff source areas can serve as focus areas for water quality monitoring, watershed management, and Best Management Practice (BMP) implementation (Walter *et al*., 2000).

The idea of delineating runoff source areas in a watershed is not new; Dunne *et al*. (1975) suggested repeated field mapping methods for catchment areas less than 8 km^2. Dunne *et al*. (1975) presented methodologies that included the use of topographic, soil and vegetative indicators to determine the extent of the runoff-producing zones for a north-eastern Vermont catchment. However, the Dunne *et al*. (1975) methodology lacked a continuous time scale, a rather important factor in the determination of hydrological parameters that influence storm runoff (Srinivasan *et al*., 2002). Anderson and Burt

* Correspondence to: I. Chaubey, Department of Agricultural and Biological Engineering and Department of Earth and Atmospheric Sciences, Purdue University, West Lafayette, IN 47907, USA.
E-mail: ichaubey@purdue.edu

(1978) presented instrumentation methods for determining runoff source areas by measuring field soil water potential. Holden and Burt (2003) mapped runoff depth for blanket peat catchments of the northern Pennines of the UK. Zollweg (1996) developed sensors to determine the soil saturation level within a 26 ha area watershed in the north-eastern USA. Srinivasan *et al*. (2000) improved upon the Zollweg sensors by automation and coupled them with surface runoff sensors to measure the temporal dynamics of runoff source areas in east-central Pennsylvania.

In this paper, a field-scale methodology is presented that identifies critical runoff source areas and dominant runoff mechanisms in a pasture watershed. This project was accomplished through the measurement of surface and subsurface field and watershed characteristics. The overall goal of this project was to understand the complexity of runoff production from a pasture watershed that overlies mantled karst geologic features.

SITE DESCRIPTION

This study was conducted on three adjacent 23 m × 23 m hillslope-plots established in Basin 1 (Figure 1) of the 1250-ha Savoy Experimental Watershed (SEW) located in north-west Arkansas, USA. The SEW serves as a multidisciplinary research site which is being used for long-term hydrologic monitoring (Brahana *et al*., 2005). Basin 1 is a 147 ha sub-basin that drains into the Illinois River. The Illinois River is a transboundary river that originates approximately 24 km south-west of the city of Fayetteville, Arkansas and flows in a north-westerly direction into Oklahoma. Land use within the Illinois River watershed is approximately 58% pasture, 36% forest and 6% urban (Soerens *et al*., 2003). The fact that Arkansas and north-west Arkansas in particular is a leader in poultry production in the USA, has led to practices such as the application of poultry litter to the soil for a long time. Over the past two decades there has been considerable controversy between the states of Oklahoma and Arkansas over the source of elevated P loadings in the Illinois River. Thus, there is a need to develop methodologies for identifying runoff- producing areas in this basin. Long-term (30 year) average annual precipitation measured in the city of Fayetteville (approximately 12 km east of the study location) was 117 cm. A low average monthly precipitation of 5 cm occurs in January and an average monthly high of 13 cm occurs in June. Winters are relatively short, with brief periods of snow cover and an average January temperature of 1 °C, whereas summers are warm and humid with an average July temperature of 26 °C (NOAA, 2002).

Land use of the SEW is representative of a typical pasture-dominated agricultural field in the Ozark Highlands. There are six major soils present immediately near and within Basin 1 with the Clarksville cherty silt loam (12–60% slope, loamy-skeletal, siliceous, semiactive, mesic Typic Paleudults) and Nixa cherty silt loam (3–8% slope, loamy-skeletal, siliceous, active, mesic Glossic Fragiudults) accounting for 79% of the area (Sauer and Logsdon, 2002). Other soils include the Pickwick silt loam (3–8% slope, fine-silty, mixed, semiactive, thermic Typic Paleudults), Razort silt loam (fine-loamy, mixed, active, mesic Mollic Hapludalfs) and Razort gravelly silt loam. The two principal soil series within the

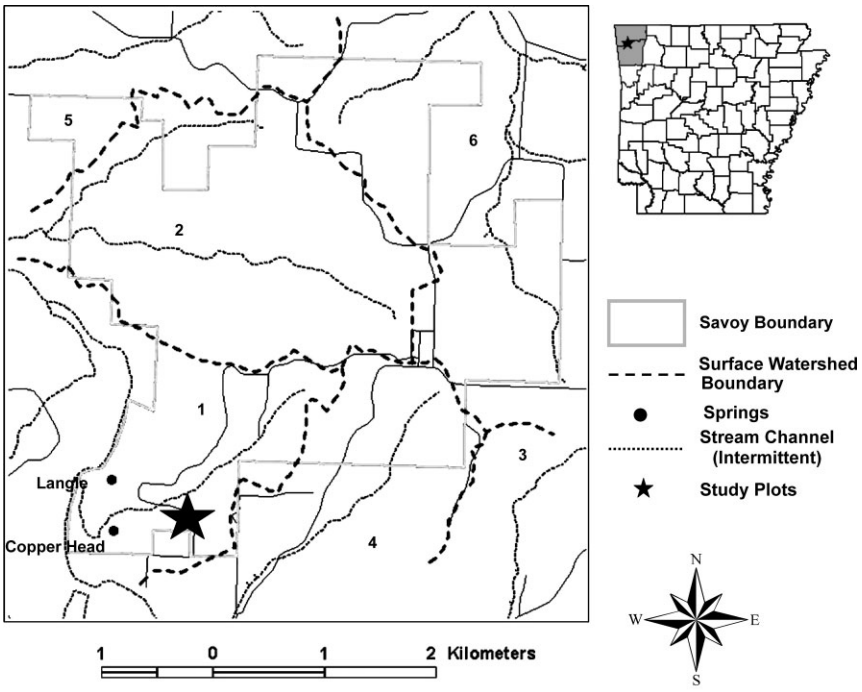

Figure 1. Location of the study site at the Savoy Experimental Watershed (SEW) in north-west Arkansas and study plots. Numbers represent surface water drainage basins

DOI: 10.1002/hyp

study plots are Captina silt loam (3–6% slope, fine-silty, siliceous, active, mesic Typic Fragiudults) and Nixa cherty silt loam. The Captina silt loam soil is typically formed on stream terraces and has strong brown subsoil that is 25–50 cm thick. Soils of the Nixa cherty silt loam typically have slow permeable fragipans that occur at the 36–60 cm depth (Harper *et al*., 1969).

INSTRUMENTATION

The three 23 m × 23 m plots (labelled plot 1, plot 2, and plot 3 in Figure 2) were bermed to isolate runoff and to prevent run-on from the upslope area. A perimeter fence with gates was constructed around the field boundary since the surrounding pastures are typically grazed. A grid of paired subsurface saturation sensors (SSS) and surface runoff sensors (SRS) (henceforth called saturation and runoff sensor, respectively) were installed at 33 points on the plots (12 on plot 1, 11 on plot 2 and 10 on plot 3 (Figure 2)). In this project, the sensors from Srinivasan *et al*. (2000) were used to quantify the dominant runoff mechanisms and identify runoff contributing areas. The saturation sensors are printed circuit boards with sensing pins that indicate the level of soil saturation at preset depths (1 cm, 5 cm, 10 cm, 20 cm, 31 cm and 46 cm). The runoff sensors are miniature v-notch weirs made of 2 mm thick galvanized sheet metal with a sensor pin and ground pin set 2 cm apart and 2·5 cm away from the v-notch, at the same level as the bottom of the v-notch. The runoff sensor

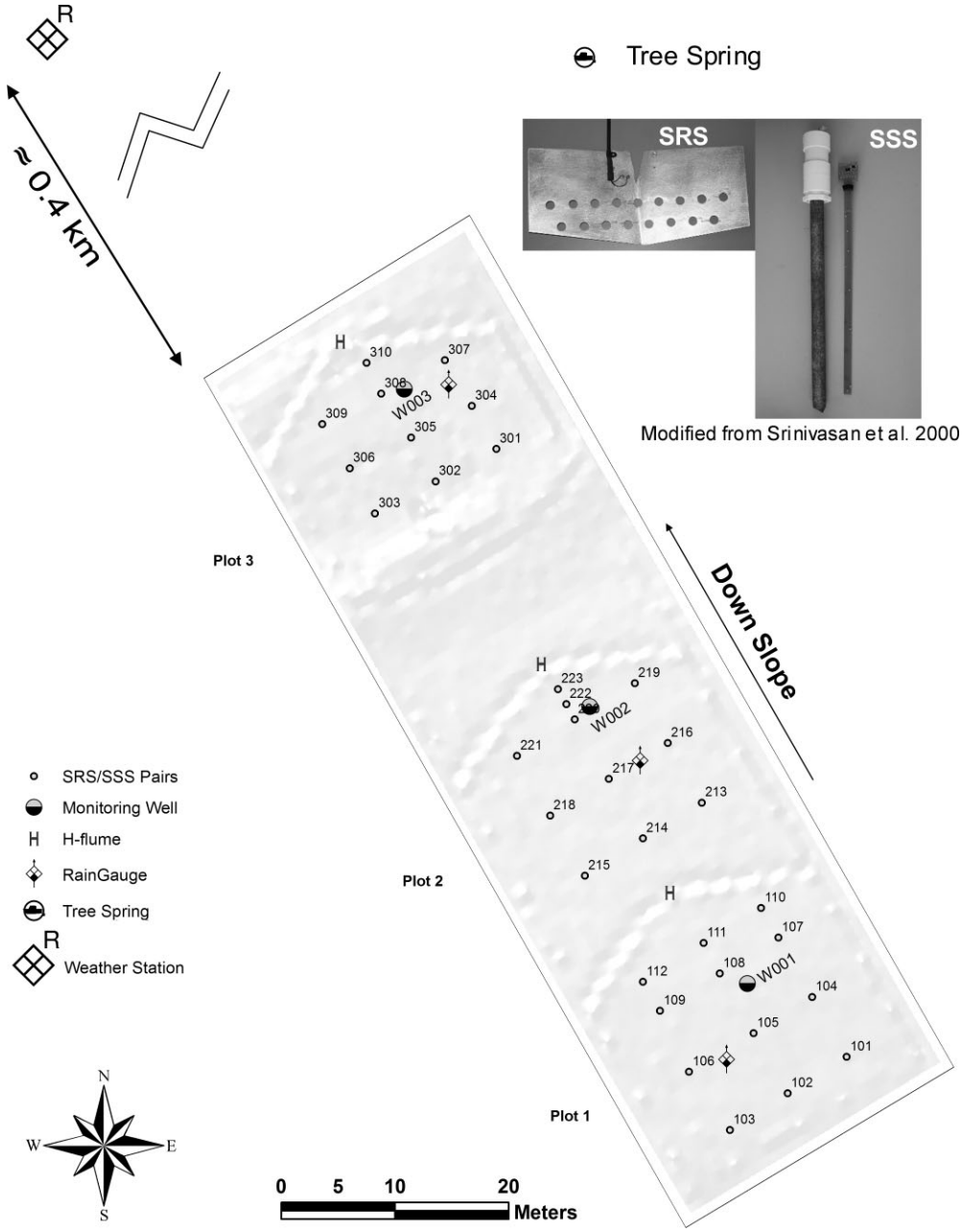

Figure 2. Site layout showing orientation and layout of data collection infrastructure including weather station, spring, rain gauges, H-flumes, surface runoff sensors (SRS) and subsurface sensors (SSS) and monitoring wells on plots 1 through 3

DOI: 10.1002/hyp

operates on a 'yes-no' basis to indicate the presence or absence of surface runoff. Full descriptions of the sensors are presented by Srinivasan *et al.* (2000).

These plots were also instrumented with a 0·305 m H-flume at the downslope end to measure the total volume of runoff from each plot. A Keller pressure transducer (Model 173, Keller America Inc., Newport News, Virgina) was used to record water depth at each flume, and the pre-determined stage–discharge relation for the flume was used to estimate runoff. It must be noted here that there is no plot-to-plot surface interaction of runoff. A 6 cm polyvinyl chloride (PVC) pipe connected a 114 L runoff collector to the H-flume at the downslope end of each plot to route surface runoff and prevent concentrated flow getting into the down slope plots. Runoff samples were collected for water quality analysis and the runoff collector subsequently emptied after each rainfall event.

A tipping bucket rain gage (HOBO RG2 model) was installed at each plot to record the spatial extent of rainfall variability. A shallow groundwater well (with a Keller pressure transducer) was installed (0·6–0·7 m deep) near each saturation sensor upslope of each H-flume to monitor depth to ground water. Locations of all infrastructures are shown in Figure 2.

All instruments were connected to a series of multiplexers and logged at 5 min intervals with a Campbell CR-23X data logger on plots 1 and 2, and a Campbell CR-10X (Campbell Scientific Inc., Logan Utah) on plot 3. Rainfall data on each plot were compared with that of a nearby weather station located approximately 0·4 km north of the study site. A spring in the northeastern corner of the plots was instrumented with a 0·152 m H-flume and a data logger.

METHODS

Topographic and Geophysical Surveys

A topography survey of the field area was determined using a high precision Global Positioning System (GPS) to obtain elevation data. The GPS survey was performed from 18 February 2004 through 23 March 2004 by establishing 1 m grid points across the plots. The grid points were georeferenced with a survey grade GPS (Leica 500 SkiPro) to the WGS 1984 coordinate system. The data obtained were processed in GIS software to obtain a 1 m resolution digital elevation model (DEM) of the field.

Surface geophysical investigations of the soil and bedrock were performed in March 2004 to characterize the subsurface attributes beneath the plots (Ernenwein and Kvamme, 2004). Two techniques (ground penetrating radar (GPR) and electrical resistance) were used to determine the underlying subsurface characteristics. In addition to seismic methods, GPR and resistance methods are the most intensively utilized techniques to map bedrock depth and integrity (Ernenwein and Kvamme, 2004).

Ground penetrating radar data collection was accomplished with a Geophysical Survey Systems International (GSSI) Subsurface Imaging Radar (SIR) 2000 system and a 400 MHz antenna. The data collection consisted of dragging the antenna across the ground surface north to south. Reflections were recorded at a rate of 32 scans per second through a range of 80 ns (two-way travel time). The GPR measurements resulted in 23 transect profiles (also known as radargrams) across the plots at 12 different depths across the hillslope. Each transect measurement was taken approximately 1 m apart and the depth measurements were at approximately 0·9 m intervals.

The resistivity survey involved introducing a weak electrical current into the ground and measuring the potential voltage. The amount of electric current that flows through the soil is directly related to soil moisture, clay content, and solutes present in the soil and rock. Electrical resistance measurements were taken every 0·5 m along parallel lines separated by 1 m with a Geoscan Research RM-15 meter. A twin-probe array with a mobile probe separation of 1 m was used to target a depth of about 1 m below the surface of the plots.

Infiltration measurements and soil physical properties

Ponded infiltration measurements were performed under relatively dry antecedent soil moisture conditions (volumetric water content $<0{\cdot}34$ cm^3 cm^{-3}). Measurements were taken on 14 June 2005 and 15 June 2005 with a double ring infiltrometer (0·15 m inner ring diameter and 0·2-m height). Three random infiltrometer measurements were made and saturated hydraulic conductivity was estimated from the final infiltration rates for each plot. The locations of the infiltration measurements were not documented. Soil core samples were taken from the 0–5 cm depth at 65 points across the plots (see Figure 6 for sampling location) to determine soil bulk density and porosity. Measurements at the 65 points were imported into a GIS software and interpolated (using an inverse weighted distance method) to derive the spatial distribution of soil properties across the plots. Statistical analyses were performed on measured values and infiltration rates using analysis of variance (ANOVA). Mean infiltration rates and bulk density were separated using Fisher's protected least significant difference test (LSD) at $P = 0{\cdot}05$.

Runoff mechanisms on the plots

Each runoff event was analysed to quantify the occurrence of saturation excess versus infiltration excess runoff on each plot. Saturation excess runoff was operationally defined as cases where the runoff sensors indicated runoff while the saturation sensors indicated a saturated soil level within 1 cm of the soil surface (surface saturation). For each event, a runoff response ratio was (RRR) defined as

$$RRR_i = \frac{\sum R_p}{n} \tag{1}$$

DOI: 10.1002/hyp

where R_p was the number of 5 min occurrences of a particular runoff process at a sensor location, and n was total number of 5 min readings taken (non-runoff events inclusive). The average *RRR* for the period of the study (2004–2005) was used to characterize the dominant runoff mechanisms that occurred.

Runoff-contributing areas

Runoff-contributing areas were quantified by interpolating runoff location points as indicated by the runoff sensors, either 1 or 0. Thus, sensor locations where runoff was known to occur were given a value of 1 and sensor locations that did not indicate runoff were assigned a value of 0. A binary map was then created by applying a threshold of 60% and above to delineate the runoff source areas. It is acknowledged that the 60% threshold is arbitrary; however, this value was arrived at empirically as a result of field observation of the area after storm events. The total percentage area contributing to runoff (A_r) during each event period was calculated as:

$$A_r = \left(\frac{\sum P_R}{P_T} \right) \times 100\% \qquad (2)$$

where P_R is the number of pixels within the delineated runoff contributing area, and P_T is the total number of pixels representing all three plots.

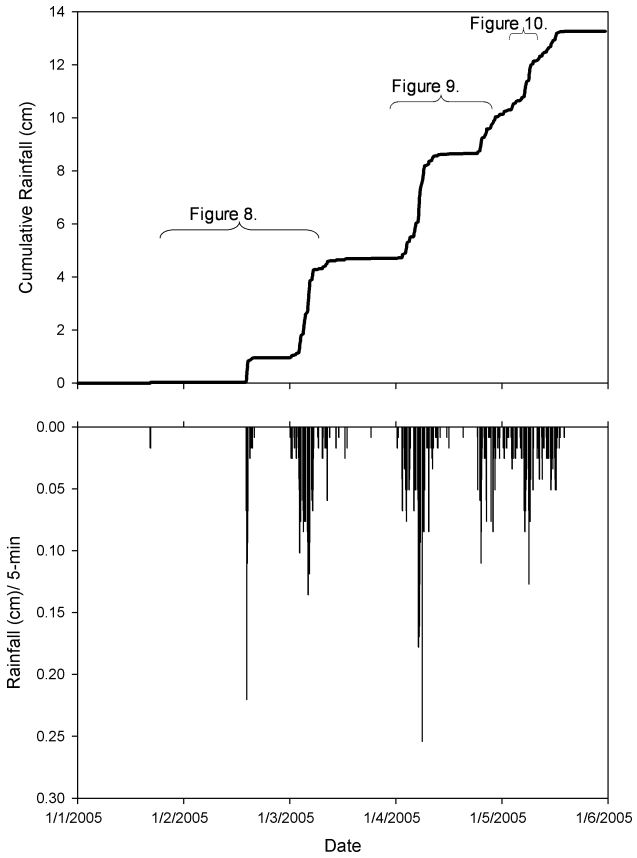

Figure 3. Cumulative rainfall and rainfall intensity in 5 min increments from 1–5 January 2005

DATA ANALYSIS

Rainfall characteristics and the plot runoff response were closely monitored from April 2004 to December 2005. In 2004, 106 precipitation events occurred, totaling 106 cm rainfall. In 2005, 111 rainfall events accounted for 95 cm of rainfall. Precipitation events within the study were defined as any 24 h period with measurable rainfall. Rainfall events that occurred 1–5 January 2005 are presented in detail in this manuscript (Figure 3). These events were selected because they revealed the unique watershed response to rainfall from a period of relatively dry watershed conditions (1–3 January 2005) to relatively wet watershed conditions (4/5 January 2005). Two weeks before the selected events, no precipitation events had occurred, with the exception of two dusting snow events that occurred on 21 and 22 December 2004. These snow events lasted only an hour and were quickly evaporated thereafter.

Sensor data were analysed to determine runoff mechanisms which occur in the field. A paired sensor analysis was used to identify the runoff mechanism that occurred. For example, the surface runoff mechanism was classified as saturation excess runoff if the saturation sensors indicated saturated soil conditions (surface saturation) and the runoff sensors indicated the presence of surface runoff. On the other hand, the runoff mechanism was classified as infiltration excess runoff if the saturation sensors did not indicate saturated conditions near the soil surface while the runoff sensors indicated the presence of surface runoff. A GIS was used to derive the spatial extent of the data and to quantify the spatial distribution of the runoff source areas. A sensor location was considered as contributing to runoff if any of the runoff mechanisms (infiltration excess or saturation excess) occurred at that particular sensor location.

RESULTS AND DISCUSSION

Topographic and geophysical surveys

The resistivity survey (Ernenwein and Kvamme, 2004) revealed a high electrical resistance (>120 Ω) area located in the southern (plot 1) to mid (plot 2) portion of the field (Figure 4). A sharp boundary of the resistance area can be seen across the end of plot 2, running from the north-east to south-west and is thought to represent regolith overlying shallow bedrock (limestone with multiple layers of bedded chert (Figure 5)).

Figure 5A shows a composite map of the GPR data at each depth sampled, and the location of sampled transect 15 (line 15). The details of transect 15 are shown in Figure 5B. In profile form, the GPR data provides a lot of detail of the nature of the subsurface characteristics of the plots. The data confirmed the findings from the resistivity survey, the upper portion of the field (plots 1 and 2) contains abundant contrasting materials (limestone,

DOI: 10.1002/hyp

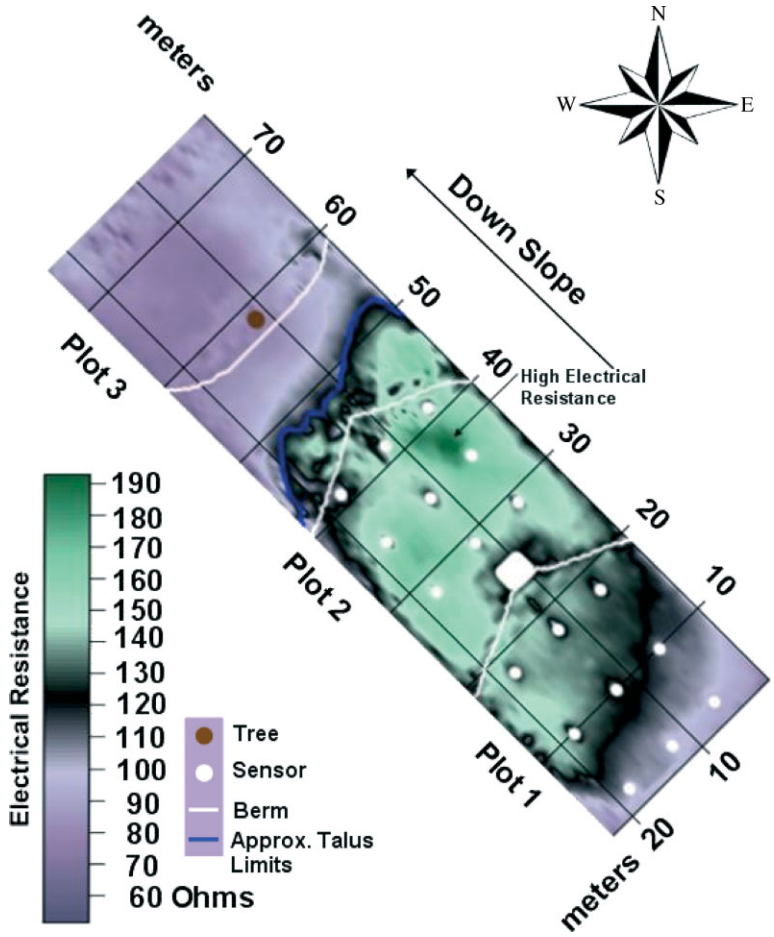

Figure 4. Electrical resistivity survey of study site showing areas of high resistance and selected sensor locations

chert, weathered zones with clay), whereas the lower portion (plot 3) is more homogenous in nature, indicating a weathered and transported regolith with a deeper zone to bedrock (Figure 5B). The resistivity data and GPR data are complementary. Combining both data sets revealed the subsurface structure of the field in great detail and was reinforced by drilling and trenching. Overall, the subsurface structure of plots 1 and 2 are interpreted as containing near-horizontal limestone bedrock with multiple layers of low-permeability chert and clay infilling bedding planes in the limestone; near-vertical fractures and probable, faults transect the plots near the berm separating plots 1 and 2, and near the northern boundary of plot 2 (Figure 5). The chert layers have been truncated by near-surface erosional processes, and are slightly tilted toward the north and west, providing a downward-stepping upper confining unit to plots 1 and 2. The chert layers are interpreted as being downfaulted beneath plot 3 (Figure 5). At Savoy, as in numerous karst areas elsewhere characterized by heterogeneous and anisotropic pathways that underdrain the soil, knowledge of the location of subsurface fractures, joints, bedding planes and distinctive soil horizons is essential to understanding the three-dimensional details of flow pathways that control runoff processes. At the study site, the limestone and chert represents the lowermost part (approximately 5 m) of the Boone Formation; the Boone is stratigraphically underlain by the St. Joe Formation, a pure limestone that is highly susceptible to dissolution and subsurface capture of infiltrated water. Continuous chert layers perch the shallow groundwater and are responsible for five small springs which lie downslope of the plots (Brahana *et al.*, 2005).

Infiltration measurements and soil physical properties

Figure 6 shows a map of the spatial distribution of bulk density on each of the plots. Mean bulk density of plot 1 (1·17 g cm^{-3}) was significantly ($P = 0{\cdot}042$) greater than the 1·01 g cm^{-3} computed for plot 3 (Figure 6). Although the mean bulk density of plot 2 was greater than that of plot 3, these differences were not statistically significant at $P = 0{\cdot}05$. Generally, bulk densities decreased from upslope (plot 1) to downslope (plot 3) of the field. The high percentage of chert on plot 1 probably accounted for the greater bulk density. The geophysical and drilling data suggest that the soil–regolith/bedrock contact is much thinner beneath plots 1 and 2 than plot 3. Although the mean bulk densities seem to be on the lower end of that reported by previous work in Basin 1 (1·10–1·46 g cm^{-3}; Sauer *et al.*, 1998; Sauer and Logsdon, 2002), the results support the general trend where Nixa cherty silt loam soils have greater bulk densities than Captina silt loams.

DOI: 10.1002/hyp

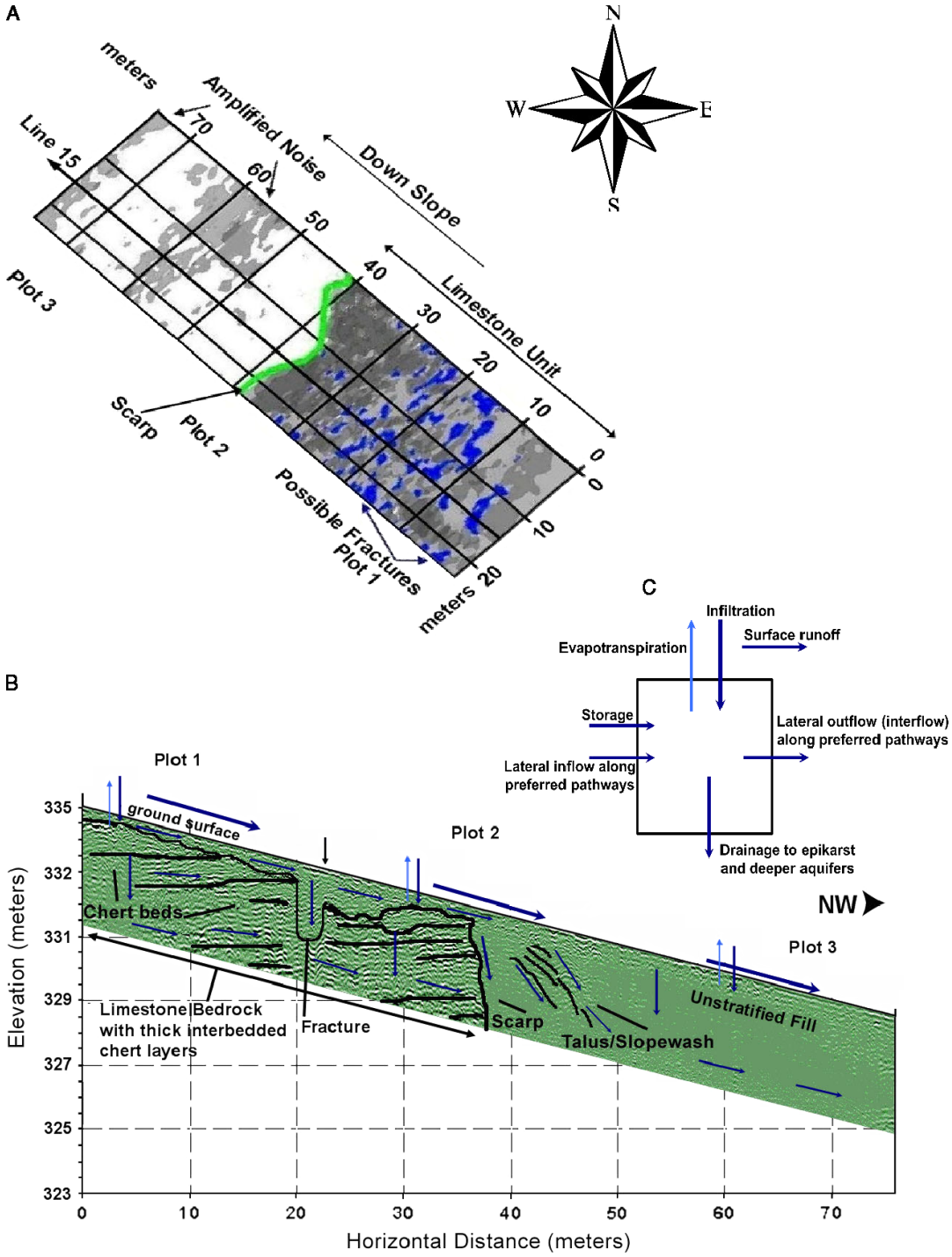

Figure 5. Conceptual model of ground penetrating radar (GPR) measurements showing (A) a composite overlay of GPR data at 12 different depths, location of transect 15, (B) details of GPR transect 15 (line 15) along with flow pathways for water, and (C) a water budget at the Savoy Experimental Watershed study plots (modified from Ernenwein and Kvamme, 2004)

Mean infiltration rate on plot 1 (302 mm h^{-1}) was significantly ($P < 0{\cdot}0082$) greater than that of plots 2 and 3 (214 mm h^{-1}). There was no significant difference between plots 2 and 3 infiltration rates (Table I). The greater infiltration rates on plot 1 could be a result of the presence of fractures in the subsurface layer of the soil, which is consistent with the resistivity and GPR surveys. These fractures could serve as macropores and induce preferential flow. Ponded infiltration rates were highly variable when compared with measurements made by other researchers on similar soil types. Infiltration rates were between ten and fifteen times greater than that reported by Sauer *et al.* (1998) (20·4 and 22·2 mm h^{-1} for Nixa and Clarksville soils respectively), between four and six times greater than values reported by Sauer *et al.* (2000) (49·0 and 54·4 mm h^{-1} for Nixa and Clarksville soils respectively) and between two and one-half times greater than values reported by Sauer and Logsdon (2002) (158 and 139 mm h^{-1} for Nixa and Clarksville soils respectively) using different infiltration

DOI: 10.1002/hyp

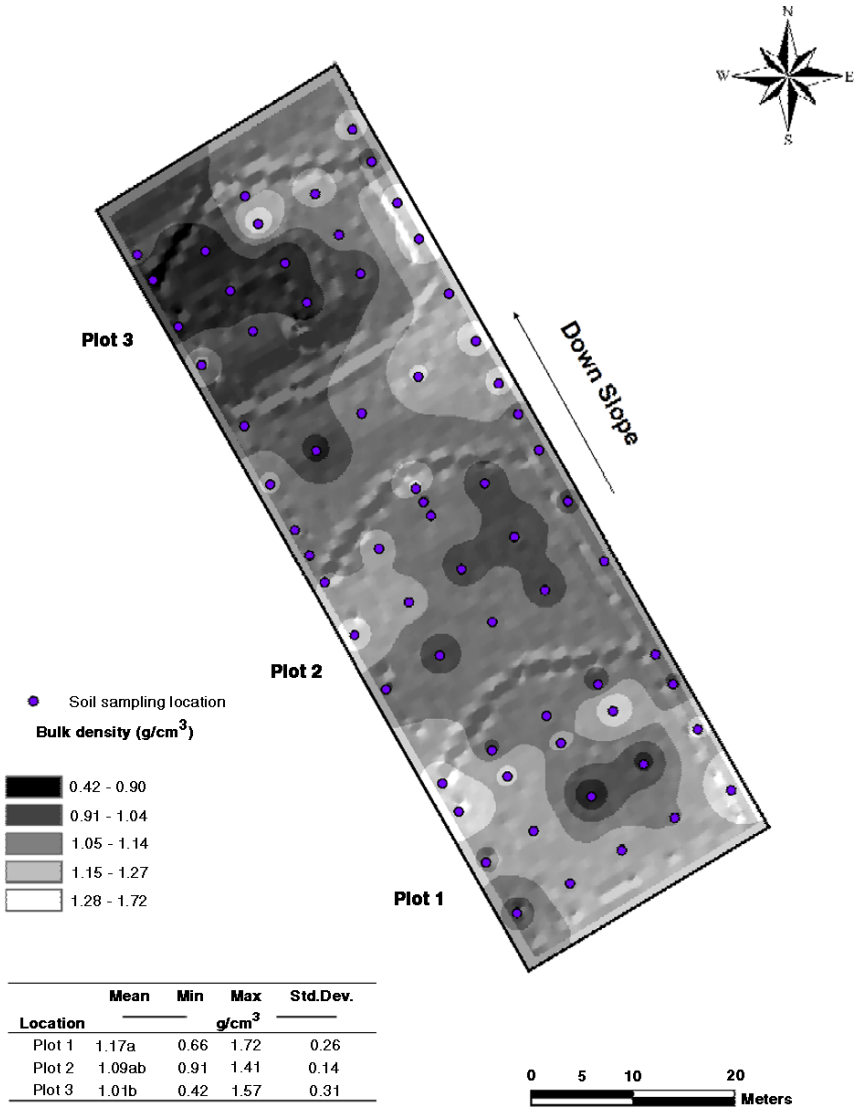

Location	Mean	Min	Max	Std.Dev.
			g/cm^3	
Plot 1	1.17a	0.66	1.72	0.26
Plot 2	1.09ab	0.91	1.41	0.14
Plot 3	1.01b	0.42	1.57	0.31

Figure 6. Spatial distribution of bulk density over study plots. Mean values followed by the same letters are not significantly different at $P = 0{\cdot}05$ as determined by Fisher's protected Least Significant Difference method

measuring techniques at a site about 0·25 km away from our study plots. Estimated infiltration rates during rainfall simulations from Haggard *et al.* (2005a) varied between 83 mm h^{-1} and 103 mm h^{-1} at small plots on a Captina silt loam. Other plot studies have observed infiltration rates of approximately 45 mm h^{-1} on a Captina silt loam variable slope box (Haggard *et al.*, 2005b). The current measured infiltration rates were on the higher side of those reported. The variability in the infiltrations rates among the different studies of similar soil types highlights the complex nature of the infiltration–runoff process in Basin 1.

Although the maximum 5 min rainfall intensities during the 1–5 January 2005 events (Table II) did not exceed the measured infiltration rates, a large number of occurrences of the infiltration excess mechanism were observed. It is possible that the variability of infiltration rates across the plots was not adequately represented since the infiltration measurements were performed at only a few (three per plot) locations on the plots. A further contribution to the high infiltration rates could be the locations of bedrock fractures underlying the subsurface soil profile (Figure 5A), or subtle elevation changes (centimetre scale) in the epikarst surface. Although not observed during this testing period, insect burrows are widespread on the plots during part of the year (John Murdoch, written communication, 2005); infiltration processes elsewhere have been documented as

Table I. Summary of infiltration measurements and estimated saturated hydraulic conductivity performed on each plot

Location	Infiltration Rate (mm/hr)		Saturated Hydraulic Conductivity (mm/hr)	
	Mean	Std Dev.	Mean	Std Dev.
Plot 1	302a*	23	173a	13
Plot 2	214b	23	116b	12
Plot 3	214b	23	120b	12

* Mean values within a column followed by the same letter are not significantly different at P = 0·05 as determined by Fisher's protected least significant difference method.

DOI: 10.1002/hyp

being dominated by macropores (Bronstert, 1999). The measurement locations were randomly chosen based on the most suitable flat surface, and the heterogeneous and anisotropic response to flow in these plots is consistent with preferred flow pathways.

Estimated saturated hydraulic conductivity on plot 1 (Table I) was significantly greater than that of plots 2 and 3 ($P < 0{\cdot}0036$). No significant difference was observed between plots 2 and 3 hydraulic conductivities. While measured saturated hydraulic conductivities were lower than values (296 mm h^{-1} for Captina soils and 312 mm h^{-1} for Nixa soils) reported by Sauer *et al*. (1998), they were between one-half and two times greater than values reported (80·2 mm h^{-1} for Nixa and 89·3 mm h^{-1} for Clarksville soils) in the Sauer and Logsdon (2002) study.

Runoff mechanisms on the plots

Both infiltration excess and saturation excess runoff occurred intermittently at the study site from April 2004 through calendar year 2005. Overall, the predominant runoff mechanism was infiltration excess, covering about 58% of the total area, and was somewhat confined to the upper portions of the hillslope (plots 1 and 2) (Figure 7). Saturation excess runoff occurs at about 26% of the total field area and appeared to be dominant on plot 3 and along the south-western boundary of plot 1. Many other researchers have documented the occurrence of saturation excess runoff near streams and at the lower portions of a hillslope (Hewlett, 1961; Dunne and Black, 1970a, 1970b; Srinivasan *et al*., 2002; Needleman, 2002; Rezzoug *et al*., 2005; Badoux *et al*., 2006). 16% of the field did not contribute to significant runoff over the period of study. It must be noted here that saturation excess runoff does occur briefly at other locations of the plots during and between storms and has a greater likelihood of occurrence during long-duration storm events.

Table II. Summary of selected rainfall characteristics and infiltration excess runoff events for 1–5 January 2005 storm events (maximum rainfall intensities in bold)

Date	Time (hours)	5-min Rainfall Intensity (cm/min)	Cummulative Rainfall (cm)	No. of 5-min Infiltration Excess Events
1/1/05	5:05 PM	<0·01	0·03	0
1/2/05	2:40 PM	0·014	0·17	3
1/2/05	2:45 PM	**0·040**	0·39	0
1/2/05	2:55 PM	0·022	0·57	2
1/3/05	2:10 AM	0·003	0·18	2
1/3/05	2:40 AM	0·020	0·47	2
1/3/05	4:30 AM	**0·027**	2·04	3
1/3/05	4:35 AM	**0·027**	2·17	2
1/3/05	4:55 AM	0·024	2·59	2
1/4/05	2:00 AM	0·010	0·08	2
1/4/05	2:40 AM	0·020	0·30	2
1/4/05	5:30 AM	0·041	1·78	8
1/4/05	5:35 AM	0·030	1·93	8
1/4/05	6:15 AM	**0·046**	2·97	15
1/5/05	5:20 AM	0·015	0·76	7
1/5/05	5:30 AM	0·010	0·84	10
1/5/05	6:30 AM	**0·025**	1·50	11

Detailed rainfall–runoff data for events that occurred from 1 January 2005 to 5 January 2005 are shown in Table III. The flow measured at the flume of plot 1 is compared with the location of runoff mechanism occurrence at different times in Table IV. Plot 1 was obviously dominated by infiltration excess, and sensor 106 (see Figure 2 for location) indicated the occurrence of saturation excess. The subsurface material could be a possible explanation for this. The presence of fractures at that location could serve as a reservoir which, when filled up, could lead to the initiation of saturation excess flow.

At 3:00 am, only sensor 104 and 106 indicated runoff. The absence of flow at the flume downslope could only suggest that the surface runoff reinfiltrated before reaching the flume. However, at 6:00 am, six sensors indicated the presence of runoff, suggesting that at least some of the runoff was able to flow downslope in order to be captured by the H-flume. A similar pattern could be observed at 10:00 am, 1:00 pm and 10:00 pm, where no flow was observed at the H-flume but the occurrence of runoff indicates reinfiltration of the runoff. Conversely, flow and corresponding runoff indication at 7:00 am, 8:00 pm and 11:00 pm suggests the runoff was able to flow to the flume via an overland flow route.

Runoff-contributing areas

The rainfall events of 1–3 January 2005 occurred after low-flow (dry) conditions were present beneath the plots (Figure 11). For a 3-week period (17–31 December 2004) before the storm of 2 January, no precipitation was recorded, except for trace amounts of snow dustings on 21 and 22 December, and base-flow recession was nearly flat. After more than 4 cm of rainfall in a period of about 48 h (Figure 3), the storms of 4/5 January 2005 (Figure 3) could be considered to have occurred under wet watershed conditions. The rainfall events of the previous days had raised the level of the groundwater table by as much as 60 to 70 cm (Figure 11) and provided well saturated soil moisture conditions. This was confirmed visually by field visits to the study site during the storm period, and are discussed in detail below.

Table III. Rainfall–runoff data for 1–5 January 2005

Date	Cumulative Rainfall (cm)		Cumulative Runoff (cm)		
	Plots*	Weather Station	Plot 1	Plot 2	Plot 3
1/1/05	0·03	0·08	0	0	0
1/2/05	0·91	0·89	0·03	<0·01	<0·01
1/3/05	3·66	3·63	0·03	0·18	0·05
1/4/05	5·39	4·83	0·13	0·69	0·13
1/5/05	3·18	2·92	0·18	0·15	0·1
5-day Total	13·16	12·34	0·37	1·02	0·28

* Mean total rainfall observed on plots 1 through 3.

DOI: 10.1002/hyp

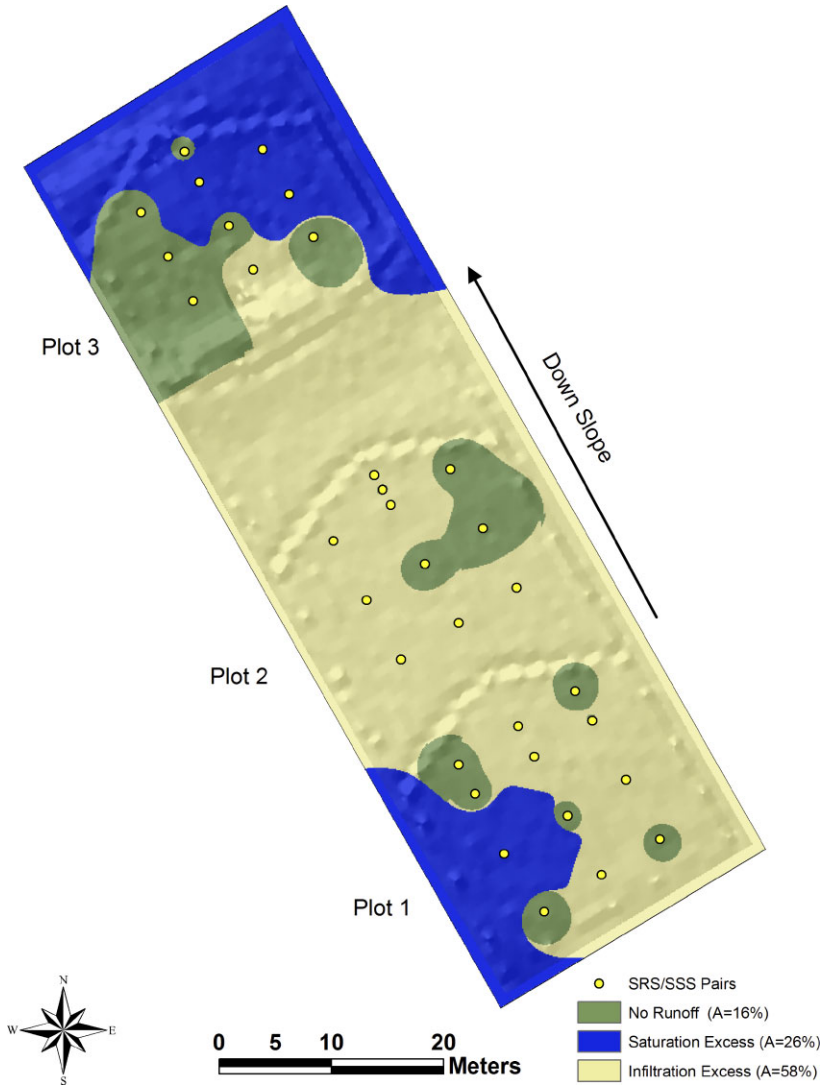

Figure 7. Map of dominant runoff process that occur at study site, Savoy, Arkansas. A is the total percentage area of a runoff process over the area of the three plots

Table IV. Flow and runoff mechanisms observed on plot 1 for 4 January 2005 event (N indicates no runoff mechanism, SE indicates saturation excess and IE indicates infiltration excess runoff)

Time (hours)	Flow measured at H-flume (m^3 s^{-1})	Sensor ID (See Figure 2 for location of sensors in plot)											
		101	102	103	104	105	106	107	108	109	110	111	112
3:00 AM	0	N	N	N	IE	N	SE	N	N	N	N	N	N
6:00 AM	1·20E-04	N	IE	N	IE	N	SE	N	IE	IE	N	IE	N
7:00 AM	7·00E-05	N	IE	N	IE	N	SE	N	IE	IE	N	IE	N
10:00 AM	0	N	N	N	IE	N	SE	N	IE	N	N	IE	N
1:00 PM	0	N	N	N	IE	N	SE	N	N	N	N	IE	N
8:00 PM	1·40E-05	N	N	N	IE	N	SE	N	N	IE	N	IE	N
10:00 PM	0	N	N	N	IE	N	SE	N	IE	N	N	IE	N
11:00 PM	5·20E-06	N	N	N	IE	N	SE	N	IE	N	N	IE	N

Runoff-contributing areas during dry watershed conditions. A minor rainfall event that occurred on 1 January 2005 was a short-duration low-intensity storm that totaled 0·03 cm (Table II, Figure 3). None of the runoff sensors responded to this event (Figure 8), nor was springflow affected (Figure 12). The 2 January event started at 2:30 pm, by 2:35 pm, three sensors had responded to the presence of runoff and 1·5% of the total area (plots 1–3) contributed to runoff (Figure 8). Rainfall intensity within this period was 0·014 cm min^{-1} and the runoff process was infiltration excess. After 10 min of the rainfall event the total infiltration excess area increased to 4%. The

DOI: 10.1002/hyp

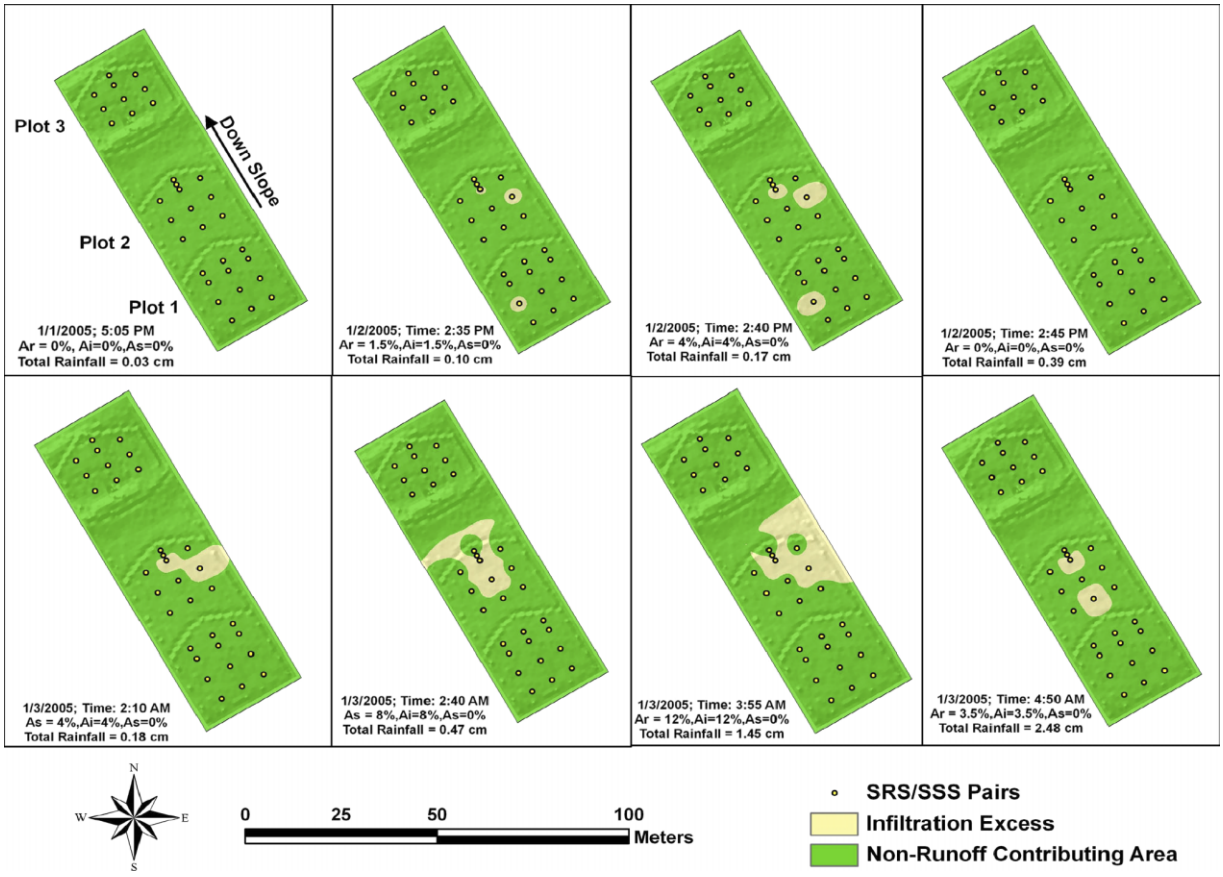

Figure 8. Map of runoff contributing areas on each plot for 1–3 January 2005 storm events. A_r is the total percentage runoff contributing area, A_i is the percentage of infiltration excess runoff area, and A_s is the percentage of saturation excess runoff area computed over all the plots

storm attained the highest intensity of 0·04 cm min^{-1} at 2 : 45 pm (Table II), but surprisingly, none of the sensors indicated the occurrence of runoff (Figure 8). Within this 5 min period, the initial runoff areas contracted, and the runoff at these sensors reinfiltrated into the soil profile; quite possibly this may be due to the development of a matric suction gradient in the relatively dry soil layers below after the soil surface had been subjected to initially wet conditions. The rainfall event ended at 4 : 15 pm with a cumulative total of 0·91 cm (Figure 3). The 3 January event started at 12 : 25 am with an intensity of 0·002 cm min^{-1}. By 2 : 10 am, the cumulative rainfall was 0·18 cm and 4% of the plots were contributing to infiltration excess runoff (Figure 8). At 2 : 40 am, the runoff contributing area had increased by 4%. The maximum infiltration excess runoff area (12%) occurred at 3 : 55 am with a cumulative rainfall of 1·45 cm and an intensity of 0·02 cm min^{-1}. The runoff-contributing areas decreased to 3·5% by 4 : 50 am with 2·48 cm total rainfall. The rainfall event ended at 5 : 55 am with a cumulative total of 3·66 cm (Table II). The absence of saturation excess runoff areas during the 1–3 January rainfall events (Figure 8) was consistent with the theory of saturation excess runoff development. The groundwater wells on each of the plots indicated water levels below the ground surface for most of the time until well 1 rose to the ground surface during the 3 January storm event. Owing to the limited spatial extent of the infiltration measurements, no conclusions can be drawn about the effects of infiltration rates; nonetheless, it is quite obvious that the higher bulk densities observed on plots 1 and 2 played a major role in the infiltration excess process during these storm events. Overall, the 1–3 January rainfall events resulted in runoff-contributing areas that were somewhat confined to plot 2 and consistent with the cumulative runoff depth that was observed on the plot (Figure 8, Table III).

Runoff-contributing areas during wet watershed conditions. The 4 January 2005 rainfall event started at 2 : 00 am (Figure 3). By 3 : 00 am, 0·33 cm of rainfall had fallen and three sensor locations indicated the occurrence of infiltration excess runoff (Figure 9). At 6·00 am 3 h later, the extent of the runoff-contributing area had increased but for the most part was confined to plots 1 and 2 (Figure 9). The groundwater well on plots 1 and 2 indicated water levels at the ground surface, while well 3 continued to rise (Figure 11) at this time. Most of the runoff (20%) produced was infiltration excess whereas only 6% of the runoff area was the result of the saturation excess mechanism. A possible explanation for the observed saturation excess areas could be macropore storage of flows in these areas (Figure 5). After a total rainfall of 3·23 cm (7 : 00 am), the maximum runoff extent (51%) was observed, 27% was due to infiltration excess and 24% was due to saturation excess mechanism. During this period, well 3 was observed to briefly rise to

DOI: 10.1002/hyp

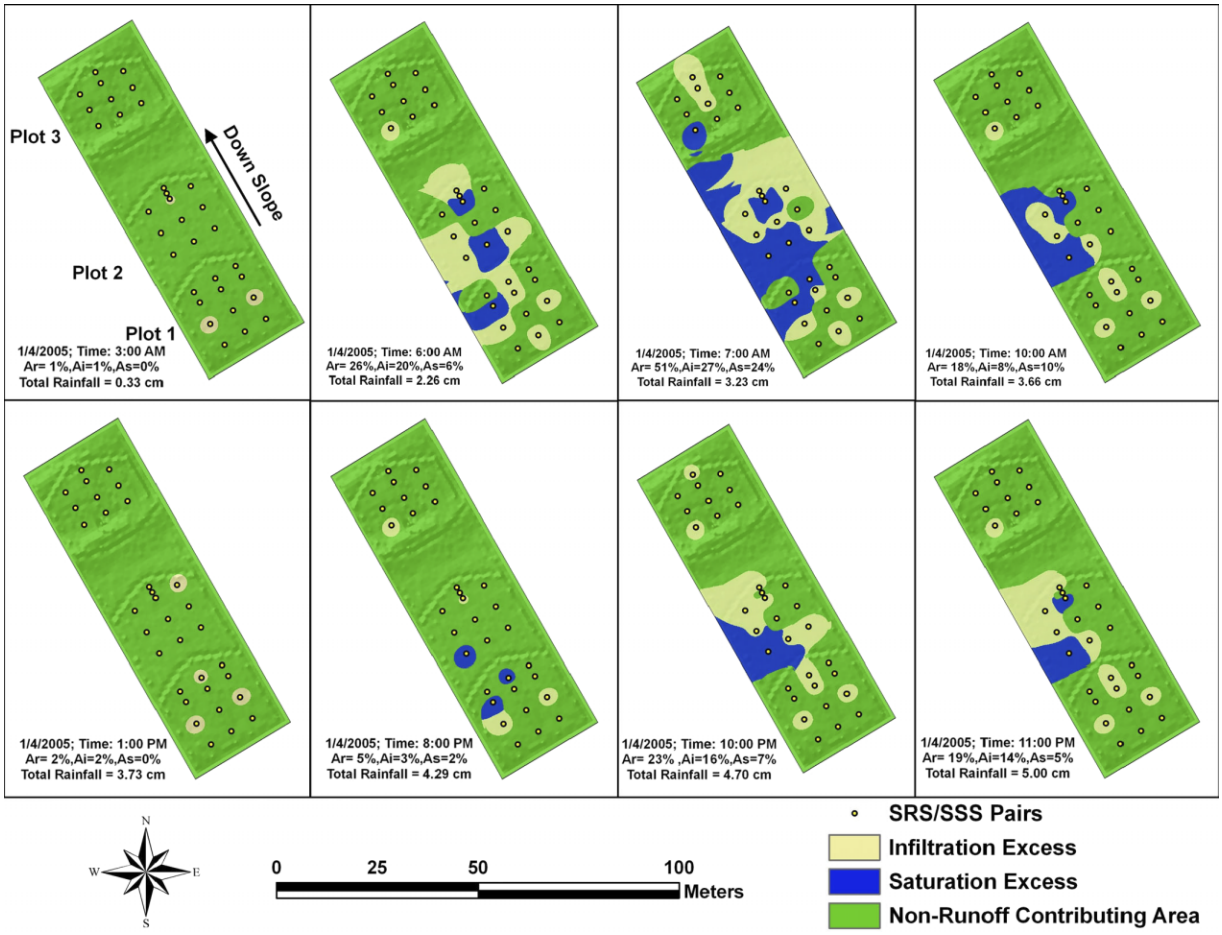

Figure 9. Map of runoff-contributing areas on each plot for 4 January 2005 storm event. A_r is the total percentage runoff contributing area, A_i is the percentage of infiltration excess runoff area, and A_s is the percentage of saturation excess runoff area computed over all the plots

ground surface. The expanded saturation excess area suggests increased storage areas in the macropores. At 10 : 00 am, the saturation excess process seemed to dominate the runoff generating process, occurring in 10% of the area whereas infiltration excess occurred in 8% of the area. The runoff areas were seen to contract to just a few spots and reverted to pure infiltration excess (2% contribution) around 1 : 00 pm. Another burst of rainfall activity, which started around 7 : 00 pm, caused the contributing areas to respond with expansion ($A_r = 23\%$, at 10 : 00 pm) and contraction ($A_r = 19\%$ at 11 : 00 pm) until midnight. Infiltration excess was the dominant runoff mechanism at both times. Both events contributed to a rainfall total of 5·39 cm at the end of the day (Table III).

The 5 January 2005 event (Figure 10) was a continuation of the 4 January late evening storm. The sensors were observed to respond to runoff by the end of the first hour (1 : 00 am) with a total runoff area of 5%, most of the runoff process being infiltration excess (4%). During that time, 0·08 cm of rainfall occurred. Two hours and 0·28 cm of rainfall later, the runoff-contributing area had increased marginally. By 6 : 00 am, a total of 1·14 cm of rain had fallen and the runoff-contributing area expanded further (Figure 10). The largest extent of runoff contribution occurred at 7 : 00 am. Within that hour, 0·64 cm of rainfall had occurred. As the rainfall amount decreased, the runoff-contributing area also decreased and by 3 : 00 pm, only the south-western part of plot 1 and south-eastern part of plot 3 contributed to runoff. Rainfall total for the storm from midnight 5 January to midnight 6 January was 3·18 cm (Figure 3). Total runoff depth was 0·18 cm for plot 1, 0·15 cm for plot 2, and 0·10 cm for plot 3. Runoff sensor 215 on plot 2 (Figure 2) indicated saturation excess runoff throughout the storm event (Figure 10). The GPR data is in conceptual agreement with this finding. The underlying chert layers have been fractured (Figure 5A) and the weathered bedrock surface of the epikarst is locally irregular with highs and lows (Figure 5B). If the subsurface drainage (Figure 5C) below areas where groundwater is perched or plugged cannot be transported rapidly, soil pores and fractures remain saturated, resulting in a saturation excess condition such as sensor 215 on plot 2 (Figure 10). The extent of the saturation excess area then depends on the amount of infiltrated water supplied to the area.

In contrast to the 4 January storm event, the 5 January storm resulted in a greater extent of saturation excess area on plot 3. This may be attributed to lateral subsurface flow from upgradient plots 1 and 2 along preferred pathways to plot 3 (Figure 5), enhancing the saturation excess generating process on plot 3.

DOI: 10.1002/hyp

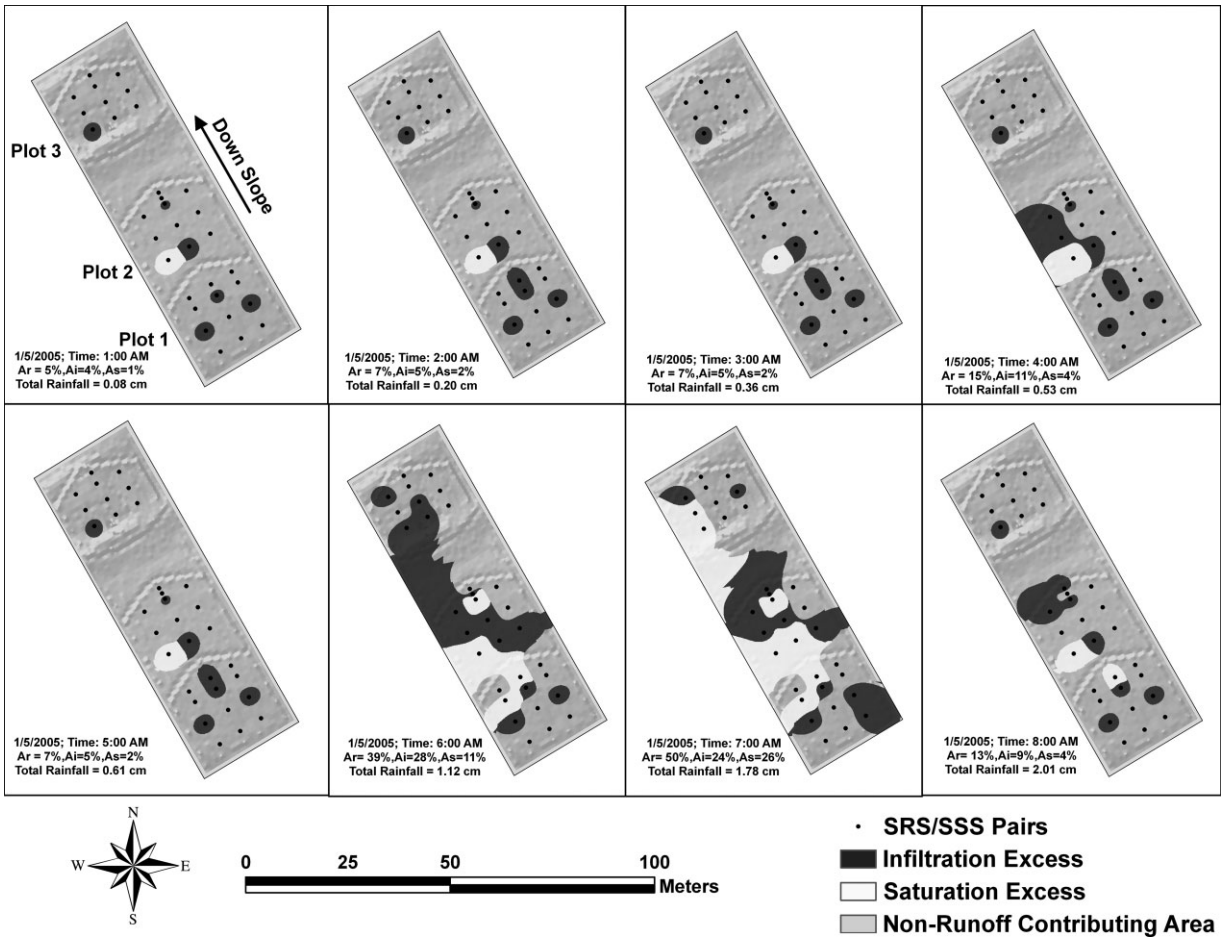

Figure 10. Map of runoff contributing areas on each plot for 5 January 2005 storm event. A_r is the total percentage runoff contributing area, A_i is the percentage of infiltration excess runoff area, and A_s is the percentage of saturation excess runoff area computed over all the plots

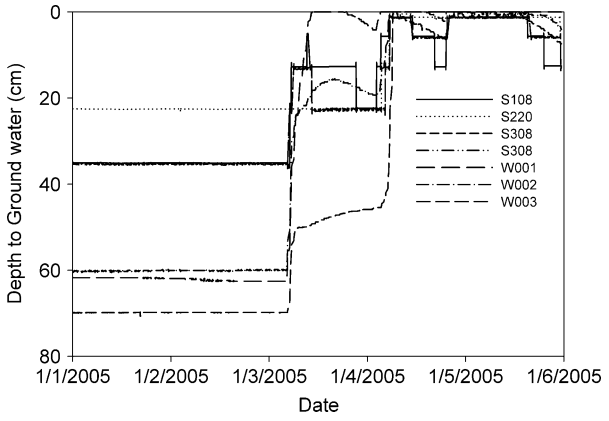

Figure 11. Water table dynamics for period 1–5 January 1 2005 as indicated by monitoring wells and nearest subsurface sensors. 'S' denotes subsurface sensors and 'W' denotes wells. Locations of subsurface sensors and monitoring wells are shown in Figure 2

Water table dynamics and flow responses

Figure 11 shows a graph of the response of the shallow monitoring wells on each plot with their corresponding nearest subsurface sensors. The subsurface sensor and monitoring well data were significantly correlated ($R^2 =$ 0·90, 0·67, 0·96 on plots 1, 2, and 3, respectively, $P <$ 0·05) and were able to capture the subsurface dynamics of the water table response to the precipitation. The time of occurrence of the relative expansion and contraction of the runoff source areas were coincident with the rise and fall of water table for the corresponding rainfall totals (Figures 3 and 8–11).

The spring flow and runoff responses to rainfall before, during, and after the 4/5 January 2005 events are shown in Figure 12. A lag in response of the spring during the 3 January storm event compared to the almost immediate response time during the 4 January storm event can be seen from this figure. Further examination of the spring hydrographs for different rainfall events revealed that the lag in spring response to rainfall is highly variable depending on rainfall intensity and antecedent soil moisture characteristics. For example, during the 2 January storm event, the spring showed a slight response 30 min after the start of rainfall but quickly receded to base flow within 15 min. For the 3 January rainfall event, spring response was observed approximately 3 h after the start of the rainfall event. However, the spring was observed to respond to the 4 January 2005 rainfall event approximately 40 min after the start of rainfall.

Examination of the groundwater wells during the dry watershed conditions is enlightening, in that the wells in plots 1 and 2 indicated low groundwater levels until the 3 January storm when they rose rapidly in response to infiltration, and after the most intense part of the storm,

DOI: 10.1002/hyp

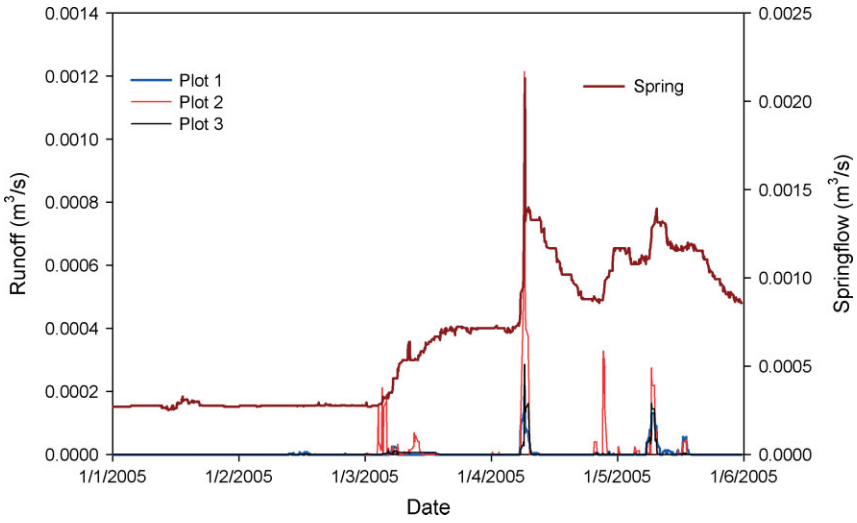

Figure 12. Spring flow and runoff on each plot for period for period 1–5 January 2005

peaked and then went into recession. The well in plot 3, however, continued rising throughout that period, until infiltration from the next storm caused a rapid rise of all wells to near ground surface the next day (Figure 11). This continual rise in well 3 is interpreted to be caused by interflow from upgradient plots 1 and 2 moving laterally along permeability contrasts in the soil zone. This lateral flow allows recession in wells 1 and 2, and continued rise in well 3. Conceptually, this is represented by dry condition flow arrows in Figure 5. Insofar as groundwater level in well 3 starts receding more steeply than the water level in well 2, it would appear that downward vertical drainage in plot 3 is more effective (more well connected) than plots 1 and 2. The wells were completed by augering to refusal, and the sequence of lithologies encountered is very similar. Thinner regolith and soil in plots 1 and 2, perched lateral interflow following the epikarst, and enhanced underdraining to the St. Joe Limestone via faults and joints represents a consistent water budget for the area, which explains most of the observed data.

For wet watershed conditions, well 1 remains nearly completely saturated after the second major pulse of infiltration through the remainder of the period of record (Figure 11). Water level rises and recessions are rapid, but the thickness of the aquifer under plot 1 between land surface and the top of the perching chert seems to be less, an observation consistent with the geophysical data and well drilling (Figure 5). Well 2 is intermediate in its response, both in timing and in magnitude, and well 3 shows the greatest transmissivity and storativity of the plots. Insofar as there is no justification that hydraulic conductivity and specific storage vary predictably over the plots, the thickness of the unconfined, porous media of the shallowest aquifer most likely is simply a result of greater thickness moving from divide to drain. Coupled with enhanced underdraining beneath fractures and faults (Figure 5B), the piling up of water in plot 2 seems like a rational consequence of interflow along preferred flowpaths and underdraining along joints and faults.

SUMMARY AND CONCLUSIONS

A field-scale methodology was used to identify and delineate runoff mechanisms and critical runoff-contributing areas in a hillslope in the Savoy Experimental Watershed. Results from this study showed that both infiltration excess and saturation excess runoff processes occur on this hillslope. Although variability of infiltration rates across the plots may not have been adequately represented, the trends in soil hydraulic properties and the subsurface attributes of the plots were instrumental in locating runoff processes in the field. The infiltration excess runoff mechanism areas were located primarily in areas of high soil electrical resistance while saturation excess mechanism areas were located in areas of subsurface fractures, low soil electrical resistance, relatively homogenous subsurface soil material, and on the downslope end of the field. The contracting and expanding dynamics of runoff generating areas were shown for five rainfall events that occurred in January 2005. Given that very little data exist on hydrologic processes and their interactions with runoff contributing areas, further study is required to develop a thorough understanding of this area of hydrology. This methodology provides a detailed procedure for capturing the hydrologic activities that occur on a hillslope and provides benchmark procedures that can be used in locating areas for best management practice (BMP) implementation.

ACKNOWLEDGEMENTS

This research project was funded by the USDA-CSREES (NRI Program) Grant No. 2003-35102-13599, USGS through Arkansas Water Resources Center (AWRC), and the University of Arkansas Division of Agriculture. The authors would also like to thank P. Srivastava, V. Garg, C. Kirkpatrick, B. Schaffer, J. Guertz, K.P. Sudheer, and K.W. Migliaccio for assistance in completing this project. Comments provided by an anonymous reviewer greatly improved earlier versions of this manuscript.

DOI: 10.1002/hyp

REFERENCES

Anderson MG, Burt TP. 1978. Toward more detailed field monitoring of variable source areas. *Water Resources Research.* **14**: 1123–1131.

Badoux A, Witzig J, Germann PF, Kienholz H, Lüscher P, Weingartner R, Hegg C. 2006. Investigations on the runoff generation at the profile and plot scales, Swiss Emmental. *Hydrological Processes* **2**: 377–394. DOI: 10·1002/hyp.6056.

Betson RP. 1964. What is watershed runoff? *Journal of Geophysical Research.* **69**: 1541–1552.

Brahana JV, Ting TE, Al-Qinna M, Murdoch JF, Davis RK, Laincz J, Killingbeck JJ, Szilvagyi E, Doheny-Skubic M, Chaubey I, Hays PD, Thoma G. 2005. Quantification of hydrologic budget parameters for the vadose zone and epikarst in mantled karst: In *Proceedings of the U.S. Geological Survey Karst Interest Group*, Rapid City, South Dakota, September 12–15, 2005, Kuniansky EL (ed). US Geological Survey Scientific Investigations, Report 2005–5160; 144–152.

Bronstert A. 1999. Capabilities and limitations of detailed hillslope hydrological modeling. *Hydrological Processes* **13**: 21–48.

Dunne T, Black RD. 1970a. An experimental investigation of runoff production in permeable soils. *Water Resources Research* **6**: 478–490.

Dunne T, Black RD. 1970b. Partial area contributions to storm runoff in a small New England watershed. *Water Resources Research.* **6**: 1296–1311.

Dunne T, Moore TR, Taylor CH. 1975. Recognition and prediction of runoff-producing zones in humid regions. *Hydrologic Sciences Bulletin* **20**: 305–327.

Ernenwein EG, Kvamme KL. 2004. Geophysical Investigations for subsurface fracture detection in the Savoy Experimental Watershed, Arkansas. Archeo-Imaging Lab unnumbered report, University of Arkansas, Fayetteville, AR, 1–48.

Freeze ET. 1974. Streamflow generation. *Reviews of Geophysics and Space Physics* **12**: 627–647.

Gburek WJ, Sharpley AN. 1998. Hydrologic controls on phosphorous loss from upland agricultural watersheds. *Journal of Environmental Quality* **27**: 267–277.

Haggard BE, DeLaune PB, Smith DR, Moore Jr PA. 2005a. Nutrient and b17-estradiol loss in runoff from various poultry litters. *Journal of American Water Resources Association* **41**: 245–256.

Haggard BE, Moore Jr PA, Brye KR. 2005b. Effect of slope on runoff from a small variable slope box-plot. *Journal of Environmental Hydrology* **13**: Paper No. 25.

Harper MD, Phillips WW, Haley GJ. 1969. Soil survey of Washington County, Arkansas. US. Department of Agriculture, Soil Conservation Service, US Government Printing Office, Washington, DC.

Hewlett JD. 1961. Soil moisture as a source of base flow seep mountain watersheds. Southeast Forest Experiment Station Paper 132. US Forest Service, US Government Printing Office, Washington, DC.

Hewlett JD, Hibbert AR. 1967. Factors affecting the response of small watersheds to precipitation in humid regions. In *Forest Hydrology*, Sopper WE, Lull HW (eds). Pergamon Press: Oxford; 275–290.

Holden J, Burt TP. 2003. Runoff production in peat covered blankets. *Water Resources Research* **39**: 1191. DOI:10·1029/2002WR001956.

Horton RE. 1933. The role of infiltration in the hydrologic cycle. *Transaction of the American Geophysical Union* **14**: 446–460.

Needleman BA. 2002. *Surface runoff hydrology and phosphorus transport along two agricultural hillslopes with contrasting soils*. PhD thesis. The Pennsylvania State University, University Park, PA.

NOAA. 2002. Climatography of the United States No. 81. Monthly station normals of temperature, precipitation, and heating and cooling degree days 1971–2000: Arkansas. Asheville, NC.

Pionke HB, Gburek WJ, Sharpley AN. 1997. Hydrologic and chemical controls on phosphorous loss from catchments. In *Phosphorous loss from soil to water*, Tunney H, Carton OT, Brookes PC, Johnston AE (eds). CAB International Press: Cambridge; 225–242.

Rezzoug A, Schumann A, Chifflard P, Zepp H. 2005. Field measurement of soil moisture dynamics and numerical simulation using the kinematic wave approximation. *Advances in Water Resources* **28**: 917–926.

Sauer TJ, Moore Jr PA, Coffeey KP, Rutledge EM. 1998. Characterizing the surface properties of soils at varying landscape positions in the Ozark highlands. *Soil Science* **163**: 907–915.

Sauer TJ, Daniel TC, Nichols DJ, West CP, Moore Jr PA, Wheeler GL. 2000. Runoff water quality from poultry litter-treated pasture and forest sites. *Journal of Environmental Quality* **29**: 515–521.

Sauer TJ, Logsdon SD. 2002. Hydraulic and physical properties of stony soils in a small watershed. *Soil Science Society of America Journal* **66**: 1947–1956.

Schindler DW, Armstrong FAJ, Holmgren SK, Brunskill GJ. 1971. Eutrophication of Lake 277, Experimental Lakes Area, Northwestern Ontario, by addition of phosphate and nitrate. *Journal of the Fisheries Research Board of Canada* **28**: 1763–1782.

Soerens TS, Fite EH III, Hipp J. 2003. Water quality in the Illinois River: Conflict and cooperation between Oklahoma and Arkansas. In *Proceedings of Diffuse Pollution Conference*, International Water Association; 14–19.

Srinivasan MS, Wittman MA, Hamlett JM, Gburek WJ. 2000. Surface and subsurface sensors to record variable runoff generation areas. *Transactions of the American Society of Agricultural Engineers* **43**: 651–660.

Srinivasan MS, Gburek WJ, Hamlett JM. 2002. Dynamics of storm flow generation-A hillslope scale field study in east-central Pennsylvania, USA. *Hydrologic Processes* **16**: 649–665.

Walter MT, Walter MF, Brooks ES, Steenhuis TS, Boll J, Weiler KR. 2000. Hydrologically sensitive areas: Variable source area hydrology implications for water quality risk assessment. *Journal of Soil and Water Conservation* **3**: 277–284.

Zollweg JA. 1996. Field study to support hydrologic modeling and analysis of watershed function at the microscale. In *Proceedings of Watershed Restoration Management—Physical, Chemical, and Biological Consideration.* American Water Resources Association; 129–134.

Zollweg JA, Gburek WJ, Pionke HB, Sharpley AN. 1995. GIS- based delineation of source areas of phosphorous within agricultural watersheds of the northeastern USA. In *Proceedings of a Boulder Symposium on Modeling and Management of Sustainable Basin-scale Water Resource Systems.* International Association of Hydrological Sciences; 31–39.